

Article

# Increasing Mechanical Properties of 3D Printed Samples by Direct Metal Laser Sintering Using Heat Treatment Process

Jozef Živčák <sup>1</sup>, Ema Nováková-Marcinčinová <sup>1,\*</sup>, Ľudmila Nováková-Marcinčinová <sup>2</sup>, Tomáš Balint <sup>1</sup>  
and Michal Puškár <sup>1</sup>

<sup>1</sup> Faculty of Mechanical Engineering, Technical University of Košice, Letná 9, 042 00 Košice, Slovakia; jozef.zivcak@tuke.sk (J.Ž.); tomas.balint@tuke.sk (T.B.); michal.puskar@tuke.sk (M.P.)

<sup>2</sup> Faculty of Manufacturing Technologies with a Seat in Prešov, Technical University of Kosice, Bayerova 1, 080 01 Prešov, Slovakia; ludmila.novakovamarcincinova@tuke.sk

\* Correspondence: ema.novakova-marcincinova@tuke.sk; Tel.: +421-055-6023543

**Abstract:** The paper deals with the evaluation of mechanical properties of 3D-printed samples based on high-strength steel powder system maraging steel using direct metal laser sintering (DMLS), which is currently being put into technical practice. The novelty of this article is that it analyzes mechanical properties of samples both printed and age hardened as well as examining the fracture surfaces. When comparing the manufacturer's range with our recorded values, samples from Set 1 demonstrated strength ranging from 1110 to ultimate 1140 MPa. Samples from Set 2 showed tensile strength values that were just below average. Our recorded range was from 1920 to ultimate 2000 MPa while the manufacturer reported a range from 1950 to 2150 MPa. The tensile strength was in the range from 841 to ultimate 852 MPa in Set 1, and from 1110 to ultimate 1130 MPa in Set 2.

**Keywords:** mechanical properties; tensile strength; laser sintering; fracture; additive technology; rapid prototyping



**Citation:** Živčák, J.; Nováková-Marcinčinová, E.; Nováková-Marcinčinová, L.; Balint, T.; Puškár, M. Increasing Mechanical Properties of 3D Printed Samples by Direct Metal Laser Sintering Using Heat Treatment Process. *J. Mar. Sci. Eng.* **2021**, *9*, 821. <https://doi.org/10.3390/jmse9080821>

Academic Editor: María Isabel Lamas Galdo

Received: 5 July 2021  
Accepted: 27 July 2021  
Published: 30 July 2021

**Publisher's Note:** MDPI stays neutral with regard to jurisdictional claims in published maps and institutional affiliations.



**Copyright:** © 2021 by the authors. Licensee MDPI, Basel, Switzerland. This article is an open access article distributed under the terms and conditions of the Creative Commons Attribution (CC BY) license (<https://creativecommons.org/licenses/by/4.0/>).

## 1. Introduction

The idea of transforming the innovative production processes from a prototype into serial production has recently become increasingly popular for many manufacturers. EOS GmbH (Electro-Optical Systems) is the global technology and quality leader for high-end solutions in the field of additive manufacturing (AM) and a global player in the field of direct metal laser sintering (DMLS). Direct metal laser sintering was developed jointly by Rapid Product Innovations (RPI) and EOS GmbH, (Electro-Optical Systems) starting in 1994 as the first commercial rapid prototyping method to produce metal parts in a single process. In addition to functional prototypes, components made by DMLS are often used for rapid tool making, medical implants, aerospace parts, and components for high-temperature environments. Additive manufacturing allows more cost-effective production for single part production, rather than batch production.

In DMLS technology, metal powder of 20 microns, free of binder or fluxing agent, is completely melted by scanning using a high-performance laser beam to form a part with original material properties. Elimination of the polymeric binder avoids the burn-off and infiltration steps and produces 95% dense steel compared to about 70% density with selective laser sintering (SLS) [1–10].

An additional benefit of the DMLS process compared to SLS is higher detail resolution due to the use of thinner layers, enabled by a smaller powder diameter. This capability allows for more intricate part shapes [1–8,11]. Material options that are currently offered include alloy steel, stainless steel, tool steel, aluminum, bronze, cobalt–chrome, and titanium [3–11]. The complexity of these parts has almost no effect on production time and costs with this technology. Complex lightweight constructions can often reduce weight and save material costs. The EOS process has proven itself in practice and can benefit from

faster and more cost-effective production: 43% shorter cooling time, 31% shorter cycle time, 43% shorter injection molding time, and functionality [4,12].

Several authors have observed mechanical properties of powder additive technologies. Recently, heat treatment methods have been used to improve these properties, where hardness and strength values have increased by more than twice [13–15], and several reports have been published on investigating the characteristics of Ti6Al4V materials produced by AM layering. The work of Brandl et al. evaluates the fatigue strength of Ti6Al4V material prepared by the laser melting process [16]. The force deformation characteristics of Ti6Al4V produced by DMLS and SLS were measured according to Facchini et al. [17]. Fatigue stress of Ti6Al4V samples produced by SLM was investigated by Van Hooreweder [18]. Liu et al. presented fatigue in Ti6Al4V samples produced by SLM, attributing weak fatigue behavior to defects [19]. Comparison of fatigue strength of samples prepared from Ti6Al4V by DMLS using the EOSINT M270 machine compared to the e-beam system was presented by Chan et al. [20]. Rafi et al. measured tensile and fatigue properties of both Ti6Al4V samples manufactured by EOS M270. Published reports on mechanical properties of high-strength steels manufactured by AM techniques are much more limited. Rafi et al. [21] and Edwards et al. [22] included DMLS materials and stainless steel in their research. The aim of the work was to evaluate mechanical properties of the newly used system of high-strength steel, to analyze the fracture surface after a static tensile test as well as to point out the redistribution of particles influenced by diversity of the chemical composition of the material used. The tests dealt with research of mechanical properties of the 3D-printed samples based on high-strength steel powder system Ti6Al4V maraging steel using direct metal laser sintering (DMLS), which is currently being put into technical practice. This research was developed based on cooperation with 1.Prešovská nástrojářeň as necessary for technical practice in order to verify and improve the properties of the mentioned material for the possibilities of better production of prototypes as well as products using the DMLS method.

## 2. Materials and Methods

### 2.1. Research Materials

The powder material from which the samples were prepared was MS1 Maraging Steel, a trademark of EOS GmbH Company. EOS Maraging Steel MS1 is a steel powder that has been specially optimized for processing on the 200W EOSINT M 280. The material composition of MS1 is listed in Table 1.

**Table 1.** Material composition.

Ni %	Co %	Mo %	Ti %	Al %	Cr, Cu %	C %	Mn, Si %	P, S %	Fe %
17–19	8.5–9.5	4.5–5.2	0.6–0.8	0.05–0.15	Each ≤ 0.5	≤0.03	Each ≤ 0.1	≤0.01	balance

Parts made of EOS Maraging Steel MS1 have chemical composition corresponding to the US classification of 18% Ni Maraging 300, European Norm 1.2709 and German X3NiCoMoTi 18-9-5. This type of steel is characterized by very good mechanical properties and is easily heat treatable using a simple hardening process to achieve excellent hardness and strength. Parts manufactured from EOS Maraging Steel MS1 are easily machined after the building process and can be easily hardened to more than 50 HRC at 490 °C (914 °F) for 6 h. In both as-built and age-hardened states, the parts can be further machined using chipping, electrical discharge machining, welding, sanding, polishing and coating, if necessary. As a result of the layer-forming method, these parts have some anisotropy, which can be reduced or eliminated by suitable heat treatment. Its mechanical properties with EOS production are listed in Tables 2 and 3.

**Table 2.** Mechanical properties of Ti6Al4V: (a) as built, only printed, (b) printed and age-hardened [9].

Density $\rho$ , g/cm <sup>3</sup>	Tensile Strength MPa		Yield Strength Rp 0.2 %		Elongation at Break % *		Modulus of Elasticity GPa *		Hardness HRC **	
	direction	XY	Z	XY	Z	XY	Z	XY		Z
8.0–8.1	(a)	1100 ± 100	1100 ± 100	1050 ± 100	1000 ± 150	10 ± 4	-	160 ± 25	150 ± 20	33–37
	(b)	2050 ± 100		1190 ± 100		4 ± 2				50–56

\* Tensile testing according to ISO 6892-1:2009. (B) Annex D, proportional test pieces, diameter of the neck area 5 mm (0.2 inch), original gauge length 25 mm (1 inch). \*\* Rockwell C (HRC) hardness measurement according to EN ISO 6508-1 on polished surface. Note that measured hardness can vary significantly depending on how the specimen has been prepared.

**Table 3.** Thermal properties of parts—Ti6Al4V [9].

	As Built	After Age Hardening ***
Thermal conductivity	15 ± 0.8 W/m °C	20 ± 1 W/m °C
Specific heat capacity	450 ± 20 J/kg °C	450 ± 20 J/kg °C
Maximum operating temperature	approx. 400 °C	

\*\*\* Ageing temperature 490 °C (914 °F), 6 h, air cooling.

The surface roughness of the material Ti6Al4V is approximately Ra = 5 µm and Rz = 28 µm with the MS1 performance method (40 µm) at MS1 surface (20 µm) Ra = 4 µm and Rz = 28 µm. Due to the layerwise building, the surface structure depends on the orientation of the surface; for example, sloping and curved surfaces are shown as a stair-step effect. These values also depend on the measurement method used. The above values indicate the difference for the horizontal orientation of the sample (upward—XY) or vertical (Z) orientation. The method used was MS1 surface and the layering was in the XY plane. Samples were prepared according to the ASTM standard for powder metallurgy technology research. Subsequently, the fracture surface of the samples was analyzed using a scanning electron microscope.

*2.2. Methods of Research*

The methodology of investigating the properties of printed materials determines and evaluates the type of high-strength steel described in the previous chapter. Tested samples were obtained by direct metal laser sintering with 3D printing in additive technologies. Two series were prepared, each with 20 samples: only printed—as-built (Set 1), and printed and age-hardened (Set 2). We followed the EOS printer manufacturer’s recommendations for the hardening process (Figure 1). Powder was also produced by the same manufacturer. The hardening process was carried out in a hardening furnace at 490 °C for 6 h; cooling was carried out in an operating room with room temperature within one day.

Strength and elongation tests were performed on samples according to ASTM standard [11] at the Technical University of Košice.

Samples were made in tool shop 1, Presovska Nastrojaren LTD, Prešov, Slovak Republic. Dimensions and shapes of the test samples are shown in Figure 2 and Table 4.

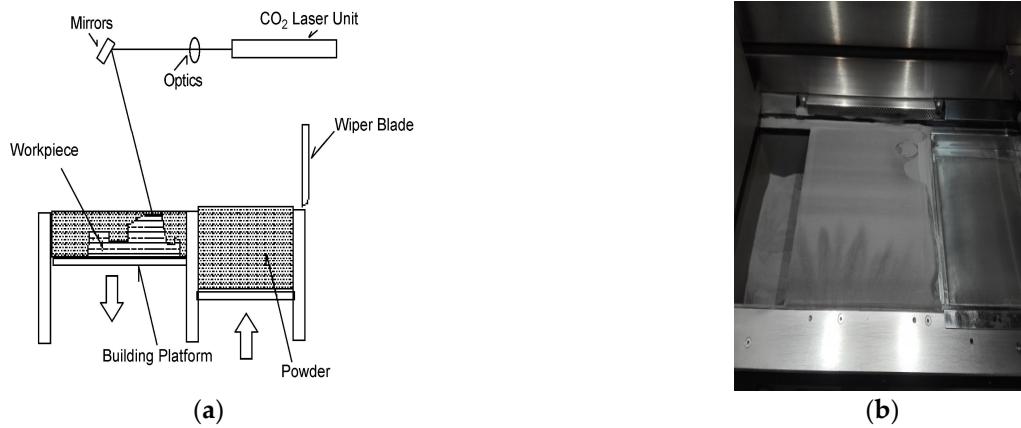


**Figure 1.** A schematic diagram [15] of the EOS Machine (a). The final sintering process in the production of samples on a DMLS 3D printer (b).

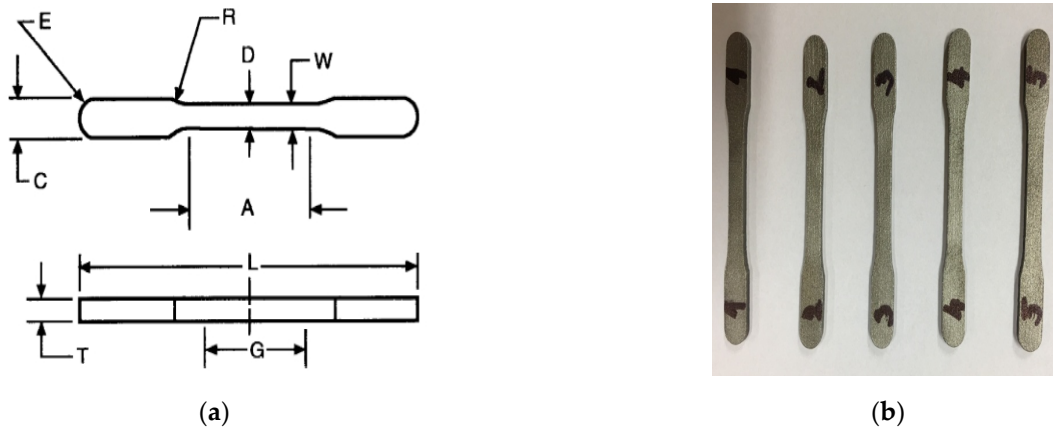


**Figure 2.** Flat unmachined tension test specimen [11] (a) and real view of samples (b) after sintering process.

**Table 4.** Dimension of tension test specimen by ASTM [10].

	Dimension [inch]	[mm]
G—Gage length	1.000 ± 0.003	25.40 ± 0.08
L—Overall length	3.53	89.7
C—Width of grip section	0.34	8.6
E—End radius	C/2	C/2
W—Width of reduced section	0.235	5.97
D—Width at center	0.225	5.72
A—Length of reduced section	1.25	31.8
R—Radius of fillet	1.00	25.4
T—Thickness	0.140 to 0.250	3.56 to 6.35

Study of the fracture surface morphology was performed on the scanning electron microscope TESCAN MIRA 3 (IMR SAS, Košice, Slovakia).

### 3. Results and Discussion

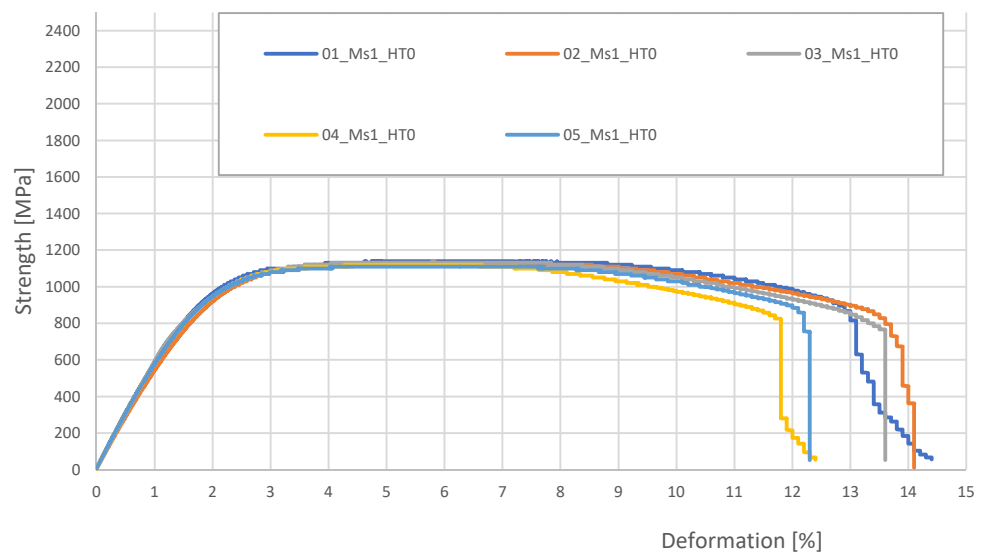
Based on the static tensile test, mechanical properties of the two series of samples of five pieces each, which are summarized in Table 5, were examined. According to ISO 6892-1 [13], the Tinius Olsen hydraulic machine was used for the tensile test. Figure 3 illustrates graphs of a portion of the tests of (a) as-built samples (Set 1) and (b) printed

and age-hardened samples (Set 2). Samples from (b) Set 2 showed a significant increase in strength values.

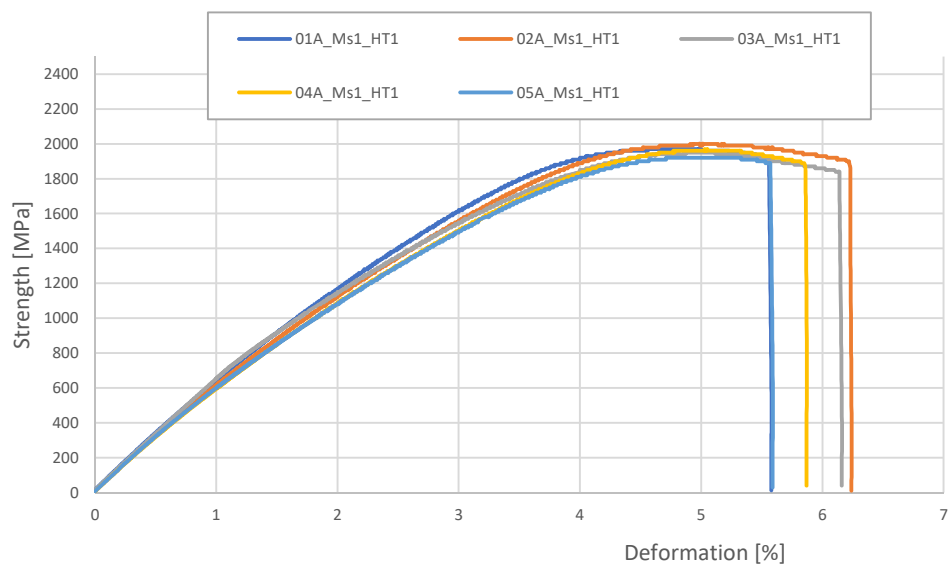
**Table 5.** Summarized mechanical properties from tensile tests.

Number of Samples	Yield Tensile Strength, MPa	Ultimate Tensile Strength, MPa	Elongation at Break %
Set 1			
Samples 1–5	841–852	1110–1140	11.1–14.3
Set 2			
Samples 1–5	1110–1130	1920–2000	2.35–3.27

Force sensor: 300 kN, speed of deformation: 0.0001 s<sup>-1</sup>.



(a) Samples of Set 1, as-built, samples 01–05 Ms1 HTD.



(b) Samples of Set 2, age-hardened, samples 01–05 Ms1 HT1.

**Figure 3.** Strength tests report.

If we compare the range given by the EOS printer manufacturer with our recorded values, the samples from Set 1 demonstrated ultimate strength ranging from 1110 to 1140 MPa. With the samples from the Set 2, the tensile strength values were only slightly below the average. Our recorded range was from 1920 to 2000 MPa, as opposed to the recommended range given by EOS of 1950–2150 MPa.

The tensile strength range was from 841 to 852 MPa in Set 1, and 1110–1130 MPa in Set 2. We can state that elongation values were within this range. The only exception was the samples from the Set 1, where the values slightly exceeded 14%. Although the hardening process is ideal for increasing hardness, as it is presented in [13,14], where hardness increased from 33 HRC to 54 HRC, elongation and tensile strength values are significantly reduced.

Fracture surface morphology was also evaluated after static tensile testing of the samples. They were observed by a scanning electron microscope and surfaces are shown in the Figures 4–6. The cross section showed a neck variation that is only visible on the printed sample (Set 1). The samples that were printed and then hardened (Set 2) demonstrated a less significant area compared to the Set 1 samples. The samples from Set 2 showed more fragile sites during surface morphology examination while the observed refractive surface of the samples from Set 1 were more plastic. In both cases, the different morphology of the whole surface was observed.

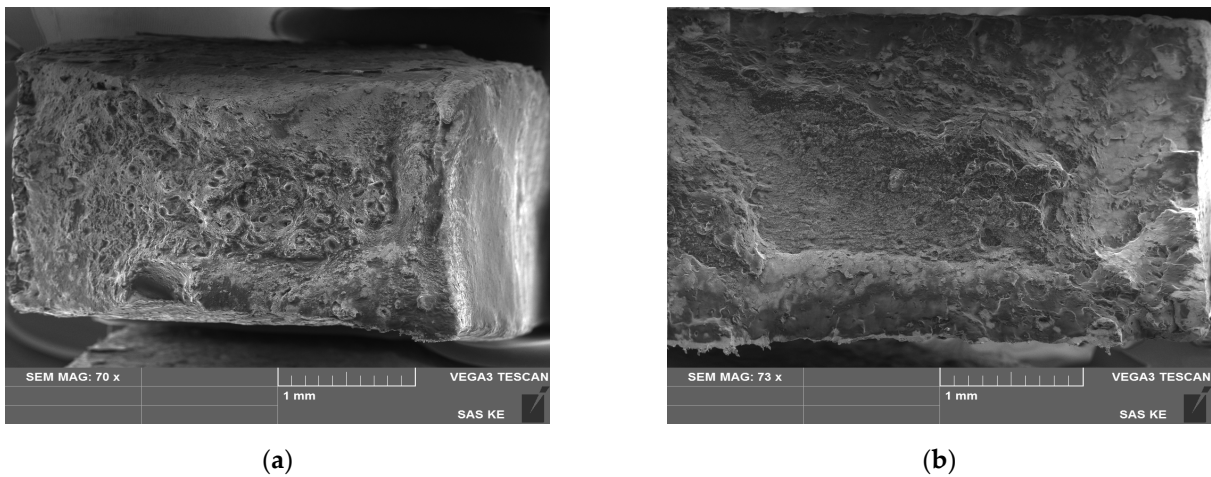


Figure 4. Surface of fracture samples: (a) Set 1, (b) Set 2 ( $\times 70$ ). Scale bar: 1 mm.

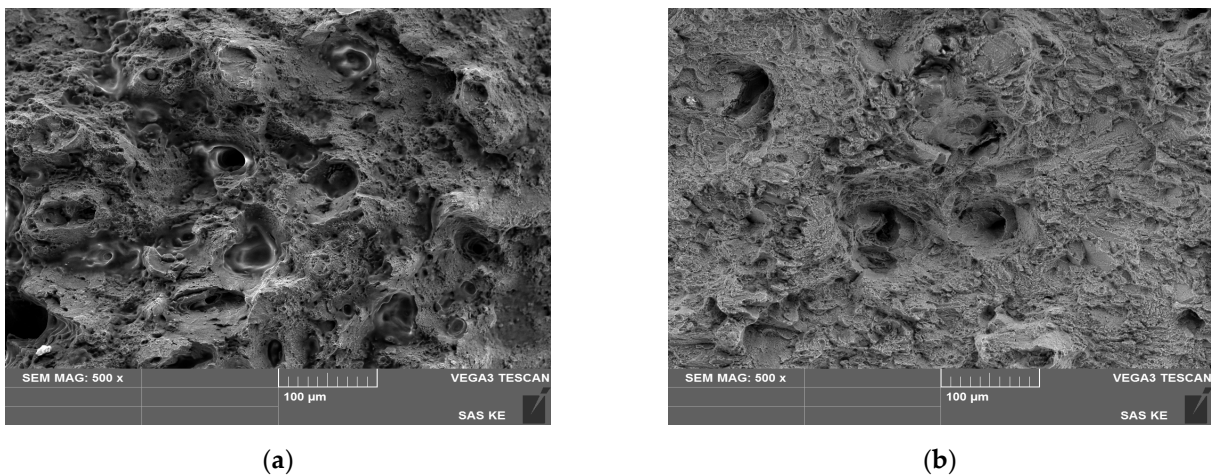


Figure 5. Surface of fracture samples: (a) Set 1, (b) Set 2 ( $\times 500$ ). Scale bar: 100  $\mu\text{m}$ .

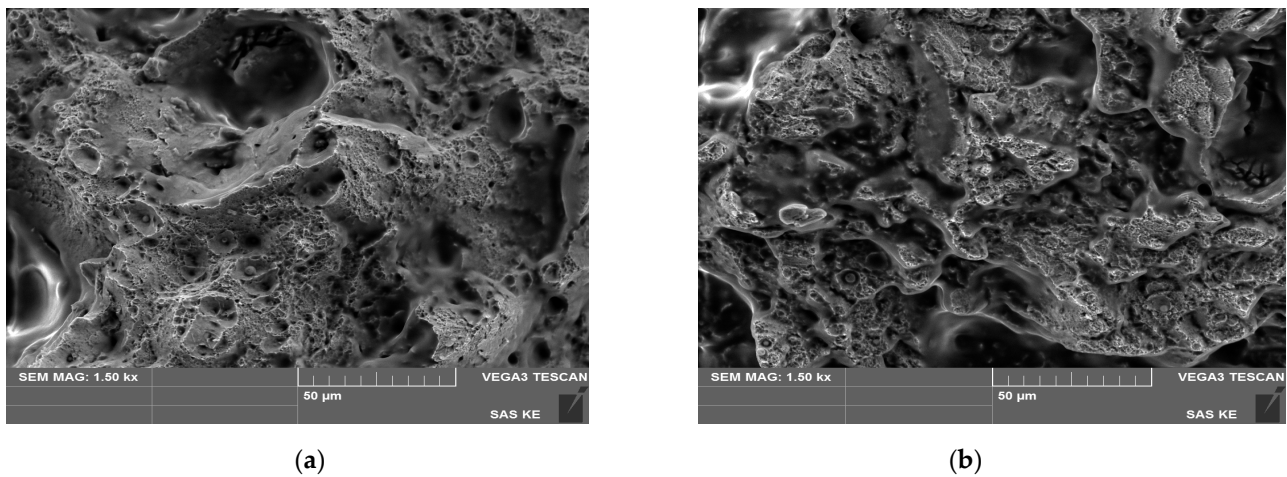


Figure 6. Surface of fracture samples: (a) Set 1, (b) Set 2 (×1500). Scale bar: 50 µm.

Table 6 presents the measured results of the chemical composition of the material Ti6Al4V of both series of samples, which were examined by EDS analysis on the evaluated fracture surfaces.

Table 6. Measured values of EDS analysis of the chemical composition of the material Ti6Al4V.

Spectrum: 1x					
El	AN	Series	unn. C [wt.%]	norm. C [wt.%]	Atom. C [at.%]
O	8	K-series	10.15	13.23	34.63
S	16	K-series	1.54	2.01	2.63
Ti	22	K-series	0.61	0.80	0.70
Fe	26	K-series	46.02	59.98	44.97
Co	27	K-series	7.32	9.54	6.78
Ni	28	K-series	11.08	14.44	10.30
Total:			76.73	100.00	100.00
Spectrum: 2x					
El	AN	Series	unn. C [wt.%]	norm. C [wt.%]	Atom. C [at.%]
O	8	K-series	11.00	13.71	36.43
Ti	22	K-series	0.62	0.78	0.69
Fe	26	K-series	46.67	58.17	44.28
Co	27	K-series	7.4	9.22	6.65
Ni	28	K-series	11.18	13.94	10.09
Mo	42	L-series	3.36	4.19	1.86
Total:			76.73	100.00	100.00
Spectrum: 3x					
El	AN	Series	unn. C [wt.%]	norm. C [wt.%]	Atom. C [at.%]
O	8	K-series	7.54	7.61	22.35
S	16	K-series	1.25	1.26	1.84
Ti	22	K-series	1.28	1.29	1.27

**Table 6.** *Cont.*

Fe	26	K-series	64.82	65.42	55.03
Co	27	K-series	11.08	11.18	8.91
Ni	28	K-series	13.11	13.24	10.59
Total:			99.09	100.00	100.00
<b>Spectrum: 4x</b>					
<b>El</b>	<b>AN</b>	<b>Series</b>	<b>unn. C</b>	<b>norm. C</b>	<b>Atom. C</b>
			[wt.%]	[wt.%]	[at.%]
O	8	K-series	7.77	7.80	23.19
Ti	22	K-series	1.25	1.25	1.24
Fe	26	K-series	64.24	64.43	54.91
Co	27	K-series	10.92	10.96	8.85
Ni	28	K-series	12.92	12.96	10.51
<b>Mo</b>	42	L-series	2.60	2.61	1.29
Total:			99.71	100.00	100.00
<b>Spectrum: 5x</b>					
<b>El</b>	<b>AN</b>	<b>Series</b>	<b>unn. C</b>	<b>norm. C</b>	<b>Atom. C</b>
			[wt.%]	[wt.%]	[at.%]
O	8	K-series	7.21	8.60	25.31
Fe	26	K-series	52.62	62.72	52.89
Co	27	K-series	8.25	9.84	7.86
Ni	28	K-series	12.66	15.09	12.11
<b>Mo</b>	42	L-series	3.14	3.75	1.84
Total:			83.9	100.00	100.00
<b>Spectrum: 6x</b>					
<b>El</b>	<b>AN</b>	<b>Series</b>	<b>unn. C</b>	<b>norm. C</b>	<b>Atom. C</b>
			[wt.%]	[wt.%]	[at.%]
O	8	K-series	8.46	9.89	28.27
Ti	22	K-series	0.66	0.77	0.73
Fe	26	K-series	52.88	61.81	50.63
Co	27	K-series	8.16	9.54	7.41
Ni	28	K-series	12.38	14.47	11.28
<b>Mo</b>	42	L-series	3.01	3.52	1.68
Total:			85.54	100.00	100.00

We have recorded the summary range mass percentage in the following range: Ti 0.69–1.27, Co 6.65–8.91, Ni 10.09–12.11, Mo 1.29–1.86. The observed Ni was below the manufacturer's reported average. The manufacturer reports 19% by weight. We have recorded that it is not exceeding 12.11% by weight. In contrast, Ti exceeded its range; it was above average. The recorded value was up to 1.27% by weight M4, while the manufacturer gives a range of up to 0.8% by weight. The difference found is fundamental for the mechanical properties of products made of this material. These different limits may cause different values of the reported mechanical properties specified by the manufacturer.

#### 4. Conclusions

The following important research results have been identified:

- Although the hardening process is ideal for increasing hardness from 33 to ultimate 54 HRC [10], elongation and tensile strength values are significantly reduced. When comparing the manufacturer's range with our recorded values, samples from Set 1 demonstrated strength ranging from 1110 to ultimate 1140 MPa. Samples from Set 2 showed tensile strength values that were just below average. Our recorded range was from 1920 to ultimate 2000 MPa while the manufacturer reported a range from 1950 to 2150 MPa. The tensile strength was in the range from 841 to ultimate 852 MPa in Set 1, and from 1110 to ultimate 1130 MPa in Set 2. The elongation values can be found to be within the range of 14% for the Set 1 samples, or slightly over 14%.
- Different limits measured in EDS chemical composition analysis may cause different values of reported mechanical properties. The observed Ni was below the manufacturer's average. We noticed that it did not exceed 12.11% by weight. Conversely, Ti exceeded its range, it was above average, recording a value of up to 1.27% by weight while the manufacturer's specified range is up to 0.8% by weight.
- The cross section of the samples showed a difference in neck that was only visible on the printed sample (Set 1). Samples that were printed and further hardened (Set 2) had a less significant area compared to the Set 1 samples. The samples from Set 2 showed more fragile areas. In contrast, the observed fracture surface of the samples from Set 1 was more plastic in both, with differences of the whole morphology.

However, despite experimentally measured values showing lower output values than the results of measurements from the material manufacturer for EOS 3D printers, it is known that these findings do not seriously affect quality of production. The strength of Ti6Al4V products can be further increased by furnace curing, like samples from the Set 2 series in our experiment. This allows unique production of form complexity and even stronger metal components than production using conformal cooling or repair of broken parts using metal powder.

**Author Contributions:** Conceptualization, J.Ž., E.N.-M. and L.N.-M.; methodology, J.Ž. and E.N.-M.; investigation, M.P., L.N.-M. and T.B.; data analysis, E.N.-M. and L.N.-M.; writing—original draft preparation, E.N.-M. and L.N.-M. and T.B.; writing—review and editing, M.P. All authors have read and agreed to the published version of the manuscript.

**Funding:** This work was supported by the Slovak Research and Development Agency under the Contract no. APVV-19-0290. The article was written in the framework of Grant Projects KEGA 041TUKE-4/2019, KEGA 006TUKE-4/2020 and the project Stimulus for research and development no. 2018/14432:1-26CO supported by the Ministry of Education of Science of Research.

**Institutional Review Board Statement:** Not applicable.

**Informed Consent Statement:** Not applicable.

**Data Availability Statement:** Not applicable.

**Conflicts of Interest:** The authors declare no conflict of interest.

#### References

1. Mancanares, C.G.; Zancul, E.D.; da Silva, J.C.; Miguel, P.A.C. Additive manufacturing process selection based on parts' selection criteria. *Int. J. Adv. Manuf. Technol.* **2015**, *80*, 1007–1014. [[CrossRef](#)]
2. Mower, T.M.; Long, M.J. Mechanical behavior of additive manufactured, powder-bed laser-fused materials. *Mat. Sci. Eng.* **2015**, *651*, 198–213. [[CrossRef](#)]
3. Nováková-Marcinčinová, L.; Novák-Marcinčin, J. Application of rapid prototyping fused deposition modelling materials. In Proceedings of the 23rd International DAAAM Symposium, Zadar, Croatia, 24–27 October 2012; pp. 57–60.
4. Nováková-Marcinčinová, L. Application of fused deposition modeling technology in 3D printing rapid prototyping area. *Manuf. Ind. Eng.* **2012**, *11*, 35–37.
5. Yasa, E.; Kruth, J.-P. Microstructural investigation of selective laser melting 316L stainless steel parts exposed to laser re-melting. *Procedia Eng.* **2011**, *19*, 389–395. [[CrossRef](#)]

6. Dzian, A.; Zivcak, J.; Penciak, R.; Hudak, R. Implantation of a 3D-printed titanium sternum in a patient with a sternal tumor. *World J. Surg. Oncol.* **2018**, *16*, 7. [[CrossRef](#)] [[PubMed](#)]
7. Findrik Balogova, A.; Hudak, R.; Toth, T.; Schnitzer, M.; Ferenc, J.; Bakos, D.; Zivcak, J. Determination of geometrical and viscoelastic properties of PLAPHB samples made by additive manufacturing for urethral substitution. *J. Biotechnol. Rev. Mol. Biotechnol.* **2018**, *284*, 123–130. [[CrossRef](#)]
8. Guzova, A.; Draganovská, D.; Ižarikova, G.; Živčák, J.; Hudak, R.; Brezinova, J.; Moro, R. The Effect of Position of Materials on a Build Platform on the Hardness, Roughness, and Corrosion Resistance of Ti6Al4V Produced by DMLS Technology. *Metals* **2019**, *10*, 1055. [[CrossRef](#)]
9. Guzanová, A.; Ižáriková, G.; Brezinová, J.; Živčák, J.; Draganovská, D.; Hudák, R. Influence of Build orientation, heat treatment, and laser power on the hardness OF Ti6al4v manufactured using The dmls Process. *Metals* **2017**, *7*, 318. [[CrossRef](#)]
10. Gál, P.; Toporcer, T.; Vidinský, B.; Hudák, R.; Živčák, J.; Sabo, J. Simple interrupted PERCUTANEOUS Suture versus Intradermal Running Suture for WOUND tensile strength measurement in Rats: A technical note. *Eur. Surg. Res.* **2009**, *43*, 61–65. [[PubMed](#)]
11. Hudák, R.; Šarik, M.; Dadej, R.; Živčák, J.; Harachová, D. Material and thermal analysis of laser sintered products. *Acta Mech. et Autom.* **2013**, *7*, 15–19.
12. Sabol, F.; Vasilenko, T.; Novotný, M.; Tomori, Z.; Bobrov, N.; Živčák, J.; Hudák, R.; Gál, P. Intradermal running Suture versus 3M™ vetbond™ Tissue adhesive for Wound closure in RODENTS: A BIOMECHANICAL and histological study. *Eur. Surg. Res.* **2010**, *45*, 321–326. [[CrossRef](#)] [[PubMed](#)]
13. Toth, T.; Hudak, R.; Zivcak, J. Dimensional verification and quality control of implants produced by additive manufacturing. *Qual. Innov. Prosper.* **2015**, *19*, 9–21. [[CrossRef](#)]
14. Tóth, T.; Živčák, J. A comparison of the outputs of 3d scanners. *Procedia Eng.* **2014**, *69*, 393–401. [[CrossRef](#)]
15. Živčák, J.; Šarik, M.; Hudák, R. FEA simulation of thermal processes during the Direct metal laser sintering of Ti64 titanium powder. *Measurement* **2016**, *94*, 893–901. [[CrossRef](#)]
16. Brandl, E.; Leyens, C.; Palm, F.; Schoberth, A.; Onteniente, P. Wire instead of powder? Properties of additive manufactured Ti–6Al–4V for aerospace applications. In Proceedings of the Euro-uRapid International Conference on Rapid Prototyping, Rapid Tooling & Rapid Manufacturing, Berlin, Germany, 23–24 September 2008.
17. Facchini, L.; Magalini, E.; Robotti, P.; Molinari, A.; Höges, S.; Wissenbach, K. Ductility of a Ti–6Al–4V alloy produced by selective laser melting of pre-alloyed powders. *Rapid Prototyp. J.* **2010**, *16*, 450–459. [[CrossRef](#)]
18. Van Hooreweder, B.; Boonen, R.; Moens, D.; Kruth, J.-P.; Sas, P. On the determination of fatigue properties of Ti6Al4V produced by selective laser melting. In Proceedings of the 53rd AIAA/ASME Structures, Structural Dynamics and Materials Conference, Honolulu, HI, USA, 23–26 April 2012.
19. Liu, Q.; Elambasseril, J.; Sun, S.; Leary, M.; Brandt, M.; Sharp, P.K. The effect of manufacturing defects on the fatigue behavior of Ti–6Al–4V specimens fabricated using selective laser melting. *Adv. Mater. Res.* **2014**, *891*, 1519–1524. [[CrossRef](#)]
20. Chan, K.S.; Koike, M.; Mason, R.L.; Okabe, T. Fatigue life of titanium alloys fabricated by additive layer manufacturing techniques for dental implants. *Metall. Mater. Trans. A* **2013**, *44*, 1010–1022. [[CrossRef](#)]
21. Rafi, H.K.; Starr, T.L.; Stucker, B.E. A comparison of the tensile, fatigue and fracture behavior of Ti–6Al–4V and 15–5 PH stainless steel parts made by selective laser melting. *Int. J. Manuf. Technol.* **2013**, *69*, 1299–1309. [[CrossRef](#)]
22. Edwards, P.; Ramulu, M. Fatigue performance of selective laser melted Ti–6Al–4V. *Mater. Sci. Eng. A* **2014**, *598*, 327–337. [[CrossRef](#)]